Thermal response and resistance optimization of various types of point-supported glass facades

Wei Lu[a], Qiangling Duan[a], Haodong Chen[b, **], Huang Li[a], Yujun Liu[a], Qingsong Wang[a], Jinhua Sun [a, *]

[a]State Key Laboratory of Fire Science, University of Science and Technology of China, Hefei 230027, China
[b]Warwick FIRE, School of Engineering, University of Warwick, Library Road, Coventry CV4 7AL, UK
* Corresponding author. Email: sunjh@ustc.edu.cn
**Corresponding author. Email: haodong.chen@warwick.ac.uk

Nomenclature

F	failure probability function
f	probability density function
m	shape factor in Weibull distribution
t	time (s) ; failure-free period (s) ; characteristic life (s)
D^*	fire characteristic diameter
δ	grid size (m)
Q	heat release rate (W)
T	temperature (K, in equation; °C, in measured data)
c	specific heat conductivity (J/(kg·K))
g	acceleration of gravity (m/s^2)
q	heat flux (kW/m^2)
k	thermal conductivity (W/(m·K))
l	decay length (m)
L	distance from the center of the holes to the edge (mm)
h	heat transfer coefficient (W/(m^2·K))
x	away lower edge (m)
y	along right edge (m)
z	dimension into glass (m)
I	absorbed incident radiative flux (kW/m^2)

Subscripts

g	glass
∞	ambient gas
0	initial
1	exposed side
2	ambient side
prediction	prediction value
max	maximum

Δ	difference
δ	glass thickness (m)
r	reference
xx	*x*-direction
yy	*y*-direction
zz	*z*-direction

Greek

ρ	density (kg/m^3)
v	Poisson's ratio
β	coefficient of linear thermal expansion (K^{-1})
E	Young's modulus (Pa)
λ	Lame coefficient
G	shear modulus (Pa)
e	volumetric strain
σ	stress (MPa); Stefan-Boltzmann constant

Abstract

The extensive application of various types of point-supported glass facades may bring potential thermal breakage risk and impacts on indoor human beings safety. In this work, point-supported glass facades with five various types were tested under thermal loads. The present results showed that installation forms influenced significantly the first breaking time, the location of crack initiation and the final falling out area. It demonstrated that the one-point-supported glass facades had the longest time for the first crack occurrence whereas the glass eventually fell completely out of the frame. However, the six-point-supported glass facades had the shortest first breaking time, but ultimately no glass pieces fell out of the frame. To calculate the temperature variation and stress distribution of glass panel, a thermal-mechanical model was developed. In addition, an optimization simulation was further conducted using the bound optimization by quadratic approximation method to obtain a better thermal resistance performance of glass facade. This work provides significant insights on the effects of various installations upon the thermal response of glass facades and helps to understand the failure mechanism and build safer facades by the structural optimization method.

Keywords: Building structural safety; Heat transfer; Point-supported glass facades; Thermal-mechanical model; Structural optimization.

Introduction

For the past few decades, glass curtain wall, as a new type of contemporary wall, which organically integrates architectural aesthetics and energy-efficient and plays an

important role in modern buildings [1] [2]. Although glass is not a kind of combustible material, it may easily break and even fall out in a fire, which will unavoidably influence building structure stability and integrity [3] and cause fire spreading [4]. Hence, the thermal resistance of building facades has a profound impact on building structural safety and its optimization is critical for structural safety design [5]. Emmons [6] highlighted that the breakage of window glass in a fire would inevitably influence the compartment fire development and building structure integrity, which has rapidly aroused widespread concern among researchers. Since then, a lot of studies concerning the thermal response of glass in theoretical models, experiments and numerical simulations have been conducted to investigate the fracture mechanism of glazing under fire condition [7]. Keski-Rahkonen [8] [9] first theoretically established heat transfer equations for rectangular and circular glass panes in a fire. According to the constitutive relation of the thermo-elasticity equation, it was concluded that the maximum tensile stress is located on the covered edge. Pagni et al. [10] [11] subsequently considered the glass absorption of radiation wavelength in the thickness direction and established one-dimensional and two-dimensional heat transfer equations, and then obtained the dimensionless temperature and stress distributions of glass panes through a semi-analytical method. On the basis of these studies, thereby, they proposed a glass breakage criterion considering the influence of shaded width which is widely used in the prediction of breaking time [12] [13]. In experimental studies. Skelly et al. [14] took the lead in designing an experimental scenario with typically layered fires in building fires and found that the critical temperature difference of edge-covered glazing was approximately 90 °C. Shields et al. [15] [16] also investigated the fire response of single and double glazing under a limited fire scenario. With regard to the numerical simulation studies, BREAK1 [17] was developed by Pagni et al. to calculate the temperature distribution of glass surface and predict the first breaking time by coupling glass breaking criterion. Kozłowski et al. [18] had established one-dimensional and two-dimensional models to precisely predict the temperature variations of monolithic and laminated glass panels under radiant heating. Thermo-mechanical performance of glass panes was investigated by Bedon et al. [19] concerning the influence of glass thickness, installation forms, fire exposure conditions, and various mechanical loads.

The prior investigations were mainly focused on edge-covered and four-point-supported glass facades [20] [21]. Nevertheless, the extensive application of various types of point-supported glass facades may bring potential fire risk. As far as we are concerned, there is a lack of comparative experimental studies on the durability of thermal response for various types of point-supported glazing systems. In consideration of the increased usage of various types of point-supported glazing, especially as the main external wall material in the external steel frame-internal

concrete tube hybrid structures of high-rise buildings, it is hence essential to investigate the breakage mechanism and specific heat transfer mechanism. These results have implications concerning fire-resistance design for glazing assemblies and could also help building designers to comply with the national fire standards.

1 Experimental Setup and theoretical principles

Figure 1 shows the experimental setup, including a propane porous rectangle burner (0.3×0.05 m^2 surface and height of 0.4 m, top surface flushed with the bottom of glass) was placed 0.25 m away from the glass facades as a fire source. A mass flowmeter with the precision of 0.01 standard L/min was adopted to control the flow rate of propane. The heat release rate (HRR) of the fire source was then calculated as the product of the mass flow rate and propane's heat of combustion (50404.55 kJ/kg). In all tests, the volume flow rate of the propane is maintained on a value of 38 L/min and thus the HRR remains in a relatively stable value of 59.28 kW. The float glass panes (600×600×6 mm^3) were installed by various types of point-supported form, including one, two, four, and six circular holes with 10 mm diameter were drilled to fix the glass panes in each corner at a distance of 55 mm from the glass edge. Glass surface temperatures were recorded by 10 K-type thermocouples with 0.5 mm diameter located in the exposed and ambient surfaces, as shown in Fig.1 (a-e). The error of temperatures determined by the thermocouples was found to be less than 3%, considering flame radiation and their diameter [22]. Water-cooled Gardon-type total incident heat flux meter with measuring range of 50 kW/m^2 (sensitivity: 0.12904mV m^2/kW) was placed in front of the exposed surface, as shown in Fig.1 (f). The detection window of heat flux meter paralleled to the exposed surface. A CCD camera (50 fps; resolution: 1920×300 pixels), an infrared camera (model: Fluke Ti 200; emissivity of glass surfaces: 0.95 [4]), and a high-speed camera (745 fps; resolution: 1920×300 pixels) were employed to record the glass breaking time, ambient surface temperatures, and dynamic breakage behavior, respectively. A change in emissivity of 0.05 would lead to a temperature variation of around 4% [4]. Therefore, the temperatures determined by the thermocouples attached to the ambient surface was applied to correct the measurements errors of IR-images. The mass of final falling out glass was measured using an electric balance (Mettler Toledo XA32001L, size: 404×360 mm^2) with an accuracy of 0.1 g. For a more intuitive description of crack initiation, points A-I represent the cracks initiated from the edge of holes. Five various types of point-supported, including one, two, four, six (vertical array), and six (horizontal array) fixed points, were investigated in the present work. Each installation type was repeated three times under a strictly controlled identical condition to ensure the accuracy and repeatability of experimental results. Despite all

the glass panels were manufactured by the same production batch and their edges were polished to the greatest extent, the uncertainties were still involved in glass physical properties [23], and thus a probabilistic approach was conducted to obtain the reference breaking time. The two-parameter Weibull function was adopted to determine the distribution of breaking time [24]:

$$F(t) = 1 - \exp\left[-\left(\frac{t}{t_0}\right)^m\right] \quad (1)$$

$$f(t) = \frac{m}{t_0}\left(\frac{t - t_u}{t_0}\right)^{m-1} \exp\left[-\left(\frac{t - t_u}{t_0}\right)^m\right] \quad (2)$$

where $F(t)$ and $f(t)$ denote the failure probability function and probability density function. m, t_u, and t_0 represent the shape factor, failure-free period, and characteristic life.

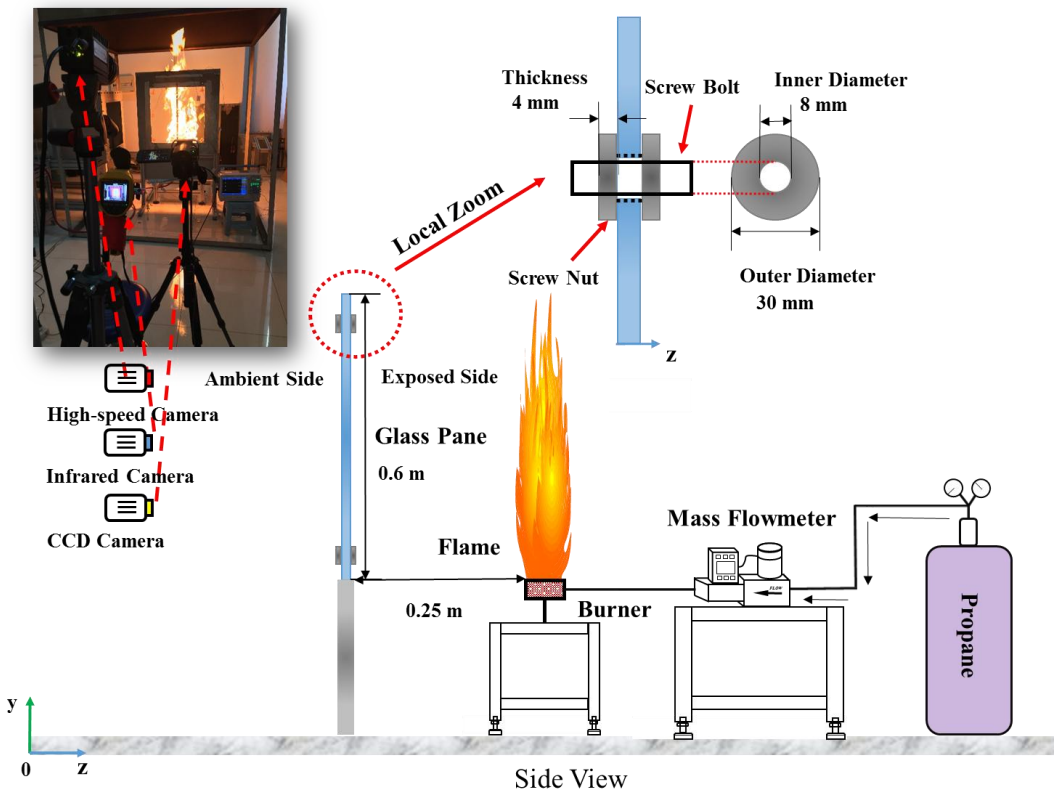

Side View

Side View

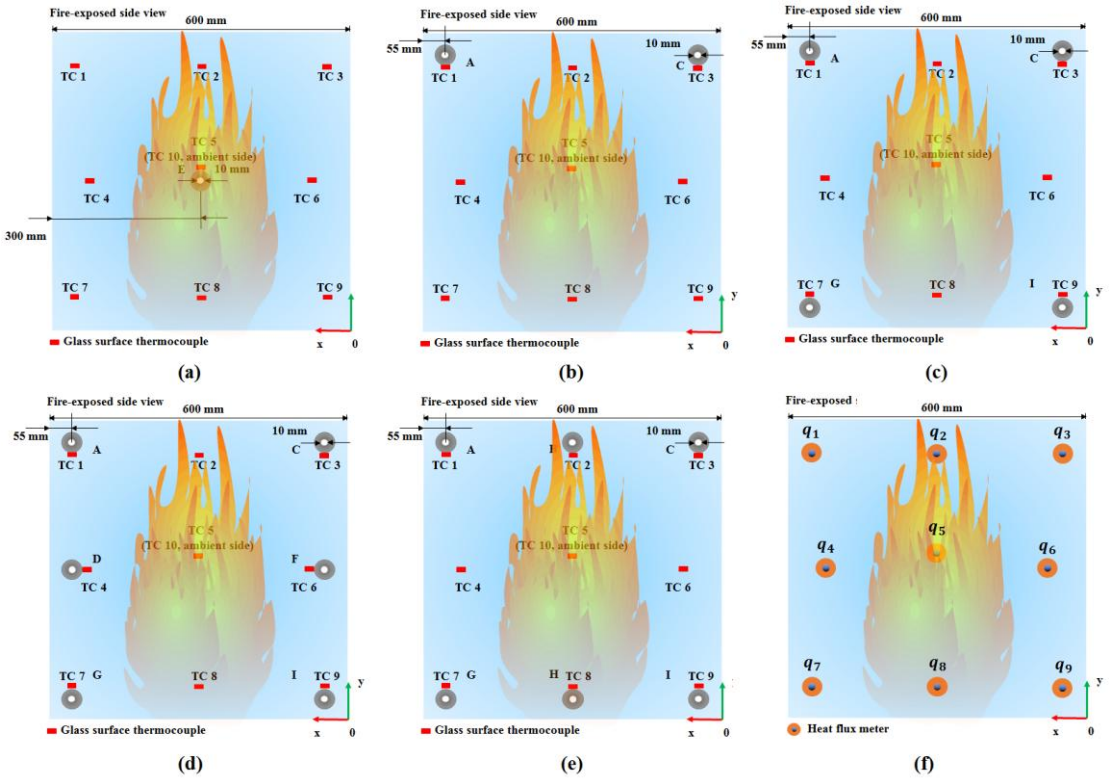

Front View

Fig. 1. Experimental and measurement setup. (a) one-point-supported; (b) two-point-supported; (c) four-point-supported; (d) six-point-supported (vertical array); (e) six-point-supported (horizontal array); (f) location of heat flux meter.

2 Numerical simulation

2.1 Heat transfer model

To understand the breaking mechanism of various types of point-supported glass facades, we simulated the temperature and stress distribution of glass panel. For revealing the heat transfer mechanism, a 3D heat transfer model was performed using a Computational Fluid Dynamics (CFD) simulation implemented in Fire Dynamics Simulator (FDS, version 6.4 with the LES model) to calculate the temperature distribution of glass panels. The sizes and physical properties of glass were identical to the experiments, as shown in Table 1.

The input of incident radiative flux directly from the flame was determined by FDS and the simulation scenario and parameters as shown in Fig. 2. The appropriate grid size ensures both simulation accuracy and time-saving. The value of fire characteristic diameter divided by grid size (D^*/δ_x) is extensively adopted to verify the resolution of the grid, and D^* is defined as follow [25]:

$$D^* = \left(\frac{Q}{\rho_0 c_0 T_0 \sqrt{g}} \right)^{2/5} \tag{3}$$

where Q is heat release rate and its value is consistent with the fire source (59.28 kW) in the experimental test. ρ_0, c_0, and T_0 represent the density, specific heat capacity and temperature of air at the initial condition (293.15 K, 100 kPa). Considering that the value of D^*/δ_x must be in the range of 4-16 [26], the mesh size with 0.02 m × 0.02 m × 0.02 m was selected based on the grid independence tests, as shown in Fig. 2.

The governing energy equation of glass panel can be expressed as [7]:

$$\rho c \frac{\partial T}{\partial t} = \nabla \cdot (k \nabla T) + I(t) \frac{e^{-z/l}}{l} \tag{4}$$

where k and c are thermal conductivity and specific heat capacity. ρ denotes density of glass. I represents the absorbed incident radiative flux that directly comes from the flame, which is determined by the radiation probes in FDS. The previous experiments suggest that the glass is absorbed by only ~ 65% of the radiation heat flux [27]. The decay length l is 0.001 m [28].

The boundary condition at the exposed surface of glass panel is given by:

$$-k \frac{\partial T}{\partial z} = h_1 \left[T_{\infty_1} - T_{g_1} \right] + \varepsilon_{\infty_1} \sigma T_{\infty_1}^4 - \varepsilon \sigma T_{g_1}^4 \tag{5}$$

At the ambient surface, the heat of glass panel dissipates into air through radiation and convection, and thus the boundary condition is written as：

$$-k \frac{\partial T}{\partial z} = h_2 \left[T_{g_2} - T_{\infty_2} \right] + \varepsilon \sigma T_{g_2}^4 - \varepsilon_{\infty_2} \sigma T_{\infty_2}^4 \tag{6}$$

where h_1 and h_2 are the convective heat transfer coefficient at the exposed and ambient surfaces which is set to 40 W/(m^2·K) [29] and 5 W/(m^2·K) [7]. ε is the emissivity of glass which is taken as 0.9 [7]. ε_{∞_1} and ε_{∞_2} denote the hot layer and cold ambient emissivity which are set to 0.0 and 1.0 [7]. T_{∞_1} and T_{∞_2} represent the gas temperature in the vicinity of the exposed and ambient surfaces which are both set to 300 K. T_{g_1} and T_{g_2} the glass temperature at the exposed and ambient surface. σ represents Steven-Boltzmann constant (σ=5.67×10^{-8} W/(m^2·K^4)).

Table 1

Thermo-physical properties of glass used in the model.

Properties	Symbol	Value
Specific heat capacity (J/(kg·K))	c	1050
Thermal conductivity (W/(m·K))	k	1.05
Poisson's ratio	v	0.22
Coefficient of linear thermal expansion (K^{-1})	β	8.55×10^{-6}
Young's modulus (Pa)	E	6.72×10^{10}

2.2 Thermal stress model

For revealing the stress field, COMSOL Multiphysics 5.3® was used to calculate the stress distribution. The grid independence tests were made to ensure the reliability of the simulation and the mesh generation in the simulation are plotted in Fig. 2. The time step was set at 1 s. The thermal stress calculation can be expressed as follow:

$$(\lambda + 2G)\nabla^2 e - \beta \nabla^2 T = 0 \tag{7}$$

where λ, G, e, and β denote the Lame coefficient, shear modulus of elasticity, a volumetric strain, and thermal expansion coefficient. λ, G, and e are expressed as follows:

$$\lambda = \frac{Ev}{(1+v)(1-2v)},\ G = \frac{E}{2(1+v)},\ e = \varepsilon_x + \varepsilon_y + \varepsilon_z \tag{8}$$

where v represents Poisson's ratio, ε_x, ε_y and ε_z denote the strain in x, y and z directions.

Due to the presence of nut at support point, the displacement of the glass in the z-direction (thickness direction) of this region is constrained. However, the constraint is not sufficient to suppress all possible rigid body displacements, so it is impossible to completely determine the displacement field. Therefore, rigid body motion suppression needs to be added to this model. The rigid body motion suppression node adds a minimum number of constraints required to suppress any rigid body modes. The constraints are selected so that there will be no reaction forces if the external loads are self-equilibrating [30].

2.3 Crack Initiation Criterion

Although the edges of the glass panes in the experiment were finely polished, the flaws were still inevitable. The critical tensile strength of glass pane is slightly different from the estimated strength because of existing flaws. In the present study, a probabilistic criterion based on a two-parameter Weibull function was used to determine crack initiation considering the randomness of glass breakage caused by flaws. A stochastic analysis of crack initiation was carried out using 20 repeated experimental results of float glass with a dimension of 600 × 600 × 600 mm^3 and the critical breaking stress was set to 60 MPa as the failure probability, $F(\sigma)$, was 0.4 [31].

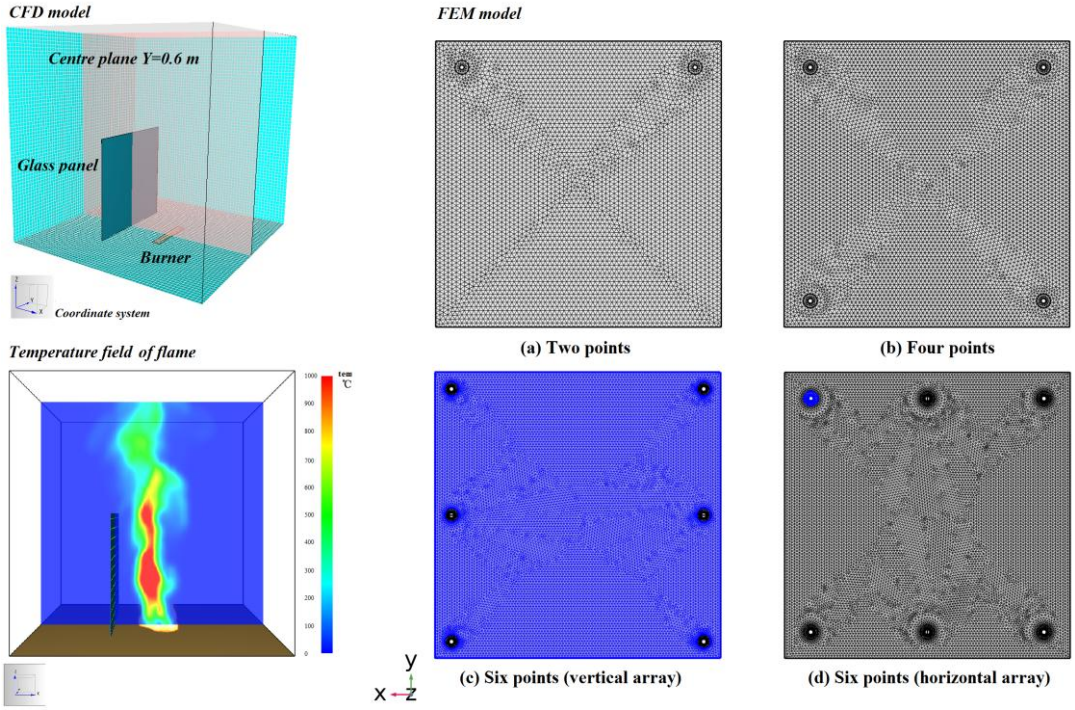

Fig. 2. The CFD model (the parameters of fire dynamics simulator: **Grid size:** 0.02 m × 0.02 m

× 0.02 m; **Burner size:** 30 cm × 5 cm; **Fuel:** propane; **Radiation fraction:** 0.3; **Combustion model:** Infinitely Fast Chemistry (Single Reaction)) and FEM model with mesh generation in simulation.

3 Experimental Results and discussion

3.1 The first breaking time and breakage behavior

A number of observations can be made for Table 2, which illustrates the breaking time, crack initiation, and final fall out ratio. A probabilistic approach was conducted to obtain the breaking time and it was assumed that the breakage time, t, satisfied two-parameter Weibull distribution and the reference breaking time, t_r, was obtained by regarding the failure probability as 0.1, as plotted in Fig. 3. It is found that the first breaking times are distributed extensively in the range of 68-421 s, indicating that the various types of installation forms have a significant influence on glass fracture behavior.

Figure 4 presents the crack evolution process and final crack path in various types of point-supported glass facades. For one-point-supported glass facade, it has the longest breaking time among the five various types of point-supported glass facades and the cracks initiation and glass fall out take place at nearly the same time within 1 s. All cracks initiate from the only central fixed point (E), and then the glass panel breaks into several pieces and finally falls out completely. Thus, it is concluded that the one-point-supported glass facade has the longest breaking time with the worst ability to maintain the integrity of the glass facades, which rapidly form a large opening to supply more oxygen for compartment fire after breakage of the glass facades and also seriously influence the stability of building structure. With regard to the two-point-supported glass facade, it is found from experiments that all the cracks initiate from the upper edge and the fixed points. The failure process is that when the cracks initiate from the upper edge and the fixed points, the panels break into two main glass pieces and then if the cracks initiate from both the two fixed points at the same time, the pieces are more prone to fall out comparing with the case that cracks only initiate from one fixed point. For tests 5 and 6, besides the cracks initiated from the upper edge, they also initiate from two fixed points (A and C), and thus the final fall out ratio is relatively larger than that in test 4, where the cracks only initiate from one fixed point (C) except the upper edge. Regarding the four-point-supported glass facade, as a common installation form, it is found that the average breaking time is 289 s and all the cracks initiate from fixed points and only a few pieces of glass fall out in Test 8, indicating that it has a better performance in maintaining glass integrity in fire than the two-point-supported glass facade. In addition, it is noteworthy that although the glass panels are both supported by six-fixed points, the fracture behavior of these two types of six-point-supported glass facade with horizontal and vertical

arrangement is quite different. It is found that the fire resistance performance of vertical arrangement is better than horizontal arrangement. For vertical arrangement, the cracks always initiate from the fixed points (D or F) on the left or right sides of the glass pane median line and rapidly form one or more approximately horizontal penetration cracks, resulting in that the glass pane breaks into two large pieces above and below. With regard to horizontal arrangement, due to the relatively larger flame radiation in the central area of the flame, the rate of temperature increase around the fixed points in the centerline area (B and H) is faster than the other points, and all cracks initiate from B or H. The specific cracks propagation process is that one or more approximately vertical cracks through the glass panel form rapidly after crack initiation, which leads to the glass panel breaking into two large pieces.

Table 2

The summary of significant parameters at the first time of glass breakage.

Installation	Test no.	First breaking time /s	Average /s	t_r /s	Crack initiation position	Final fall out ratio /%
One point	1	410	412	395	E	100
	2	404			E	100
	3	421			E	100
Two points	4	259	261	257	upper edge, C	48.75
	5	262			upper edge, A, C	67.21
	6	263			upper edge, A, C	97.62
Four points	7	278	289	265	A, G	0
	8	291			I	3.75
	9	300			A, C, I	0
Six points (vertical array)	10	105	111	100	F	0
	11	117			F	0
	12	110			D	0
Six points (horizontal array)	13	83	76	63	H	0
	14	78			B	0
	15	68			H	0

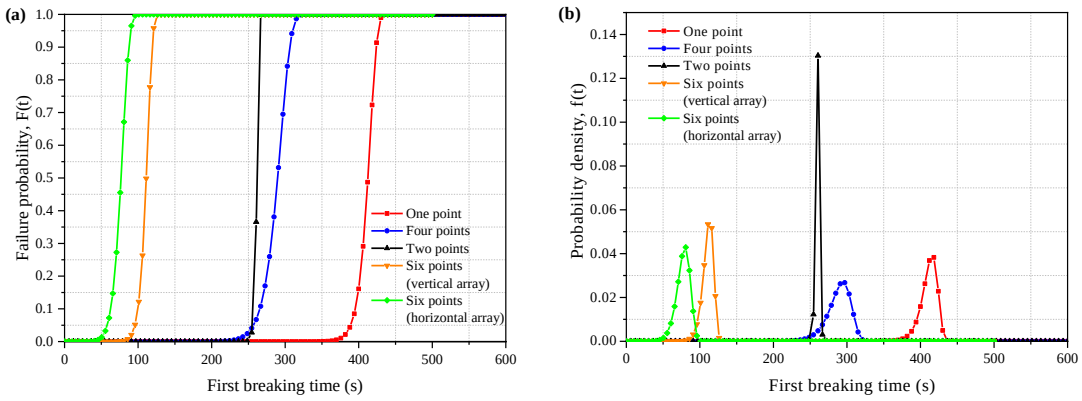

Fig. 3. The two-parameter Weibull distribution results at the first breaking time, (a) the failure probability function, and (b) the probability density function.

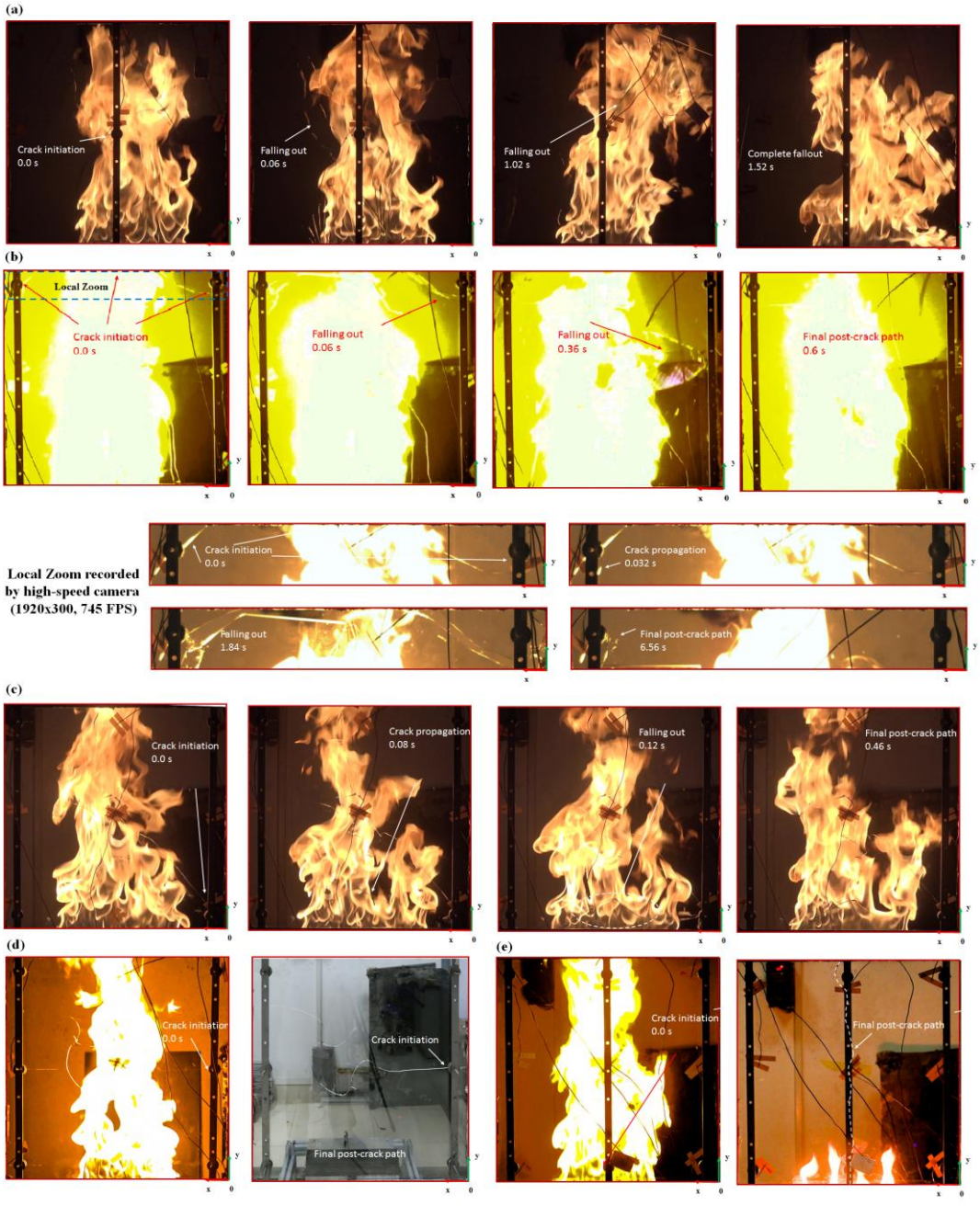

Fig. 4. The crack evolution process and final crack path in Tests 2, 6, 8, 10, and 13.

3.2 Glass surface temperature and total heat flux

Both contact and non-contact methods were applied to obtain the temperature of the glass surface. Figure 5 illustrates the variation of the temperatures measured by thermocouples (TCs) at different monitoring points and the infrared image at the first breaking. It is found that the temperature measured by TC 5 is the highest and increases with the increase of breaking time. The infrared image at the moment of the first breaking visually demonstrates the temperature distribution is in good agreement with the size and location of the fire source, and as time increases, the high-temperature region at the center of glass expands further. We established a simple glass surface temperature prediction model by assuming the glass pane to be a thermal lump and using an energy balance equation as follows [16]:

$$\rho c\delta \frac{dT_g}{dt} + h_2 \left(T_g - T_{\infty_2}\right) = q \tag{9}$$

Under this case, due to the relatively stable HRR of propane burner, it is assumed that the total incident heat flux q is constant which is set to the average measured value during the experiments and convective heat transfer coefficient h_2 is set to 50 W/(m^2·K) for the breaking time above 250 s (high-temperature region) and 5 W/(m^2·K) for the breaking time below 120 s (low-temperature region) and then the following expression can be calculated, relating the glass temperature, by solving the above ordinary differential equation.

$$T_g = q\left(\frac{1 - e^{-\frac{h_2}{\rho\delta c}t}}{h_2}\right) + T_{\infty_2} \tag{10}$$

Due to the various intensity of the flame radiation, the measured temperatures at the centerline are relatively higher than the left and right sides. In general, thermal stress that caused the glass breaking is generated by the temperature gradient [6]. As the temperature gradient increases, the breaking occurs when the thermal stress exceeds the critical tensile stress of glass pane. To determine the temperature gradient at breaking time, the temperature difference is defined as follows:

$$\Delta T = \frac{T_2 + T_5 + T_8}{3} - \frac{T_1 + T_3 + T_4 + T_6 + T_7}{6} \tag{11}$$

$$\Delta T_{prediction} = \left(\frac{q_2 + q_5 + q_8}{3} - \frac{q_1 + q_3 + q_4 + q_6 + q_7 + q_9}{6}\right)\left(\frac{1 - e^{-\frac{h_2}{\rho\delta c}t}}{h_2}\right) \tag{12}$$

where T_i donates the temperature obtained by TCi. q_i represents the total incident heat flux measured at which the corresponding TCs are located and then $\Delta T_{\text{prediction}}$ can be calculated through bring equation (10) into equation (11). Figure 6 (a) illustrates the

predicted temperature difference $\Delta T_{\text{prediction}}$ at the exposed surface. The test results are indicated by the *x*-axis and the calculation results are by the *y*-axis. Points which falls on the diagonal line signifies that it completely consistent with the tests, and data points in the upper and lower triangle zones suggest over-prediction and under-prediction. Two control lines with a relative error of ± 10% and ± 30 % are plotted, as a reflection of prediction accuracy. The temperature predictions seem to be more consistent with the test results for breaking time above 250 s, while they are smaller than the test results for the breaking time below 120 s. Furthermore, the discrepancy between the theoretical calculation and the test results decreases as the breaking time increases from 68 to 421 s.

Figure 6(b) demonstrates that the value of ΔT is a distinct difference among various types of point-supported glass facades, which further suggests the significant influence of installation form on the performance of fire-resistance. It is found that the average value of ΔT at the exposed surface also increases with the increase of breaking time. In addition, ΔT_{max} denotes the maximum temperature difference at glass ambient surface obtained by the infrared image at breaking time and it is concluded that the average value of ΔT_{max} increases with the increase of breaking time, which demonstrates that the temperature difference can be a criterion to determine the occurrence of glass breakage for various types of point-supported glass facades.

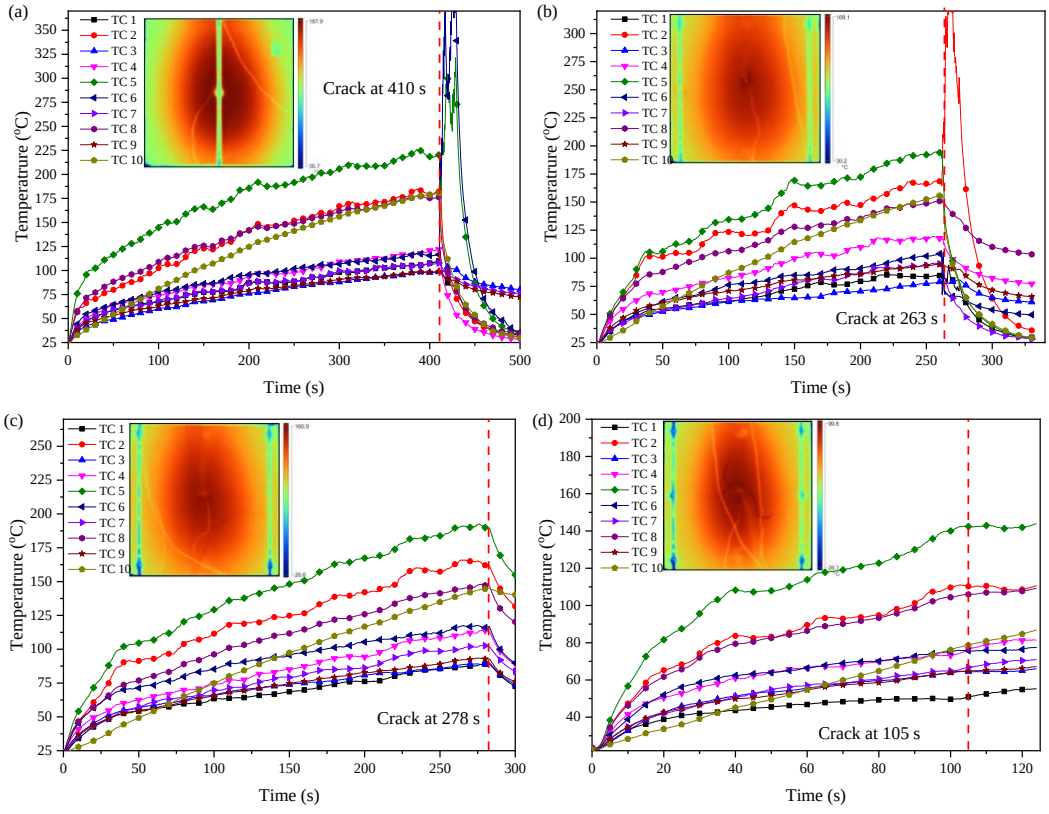

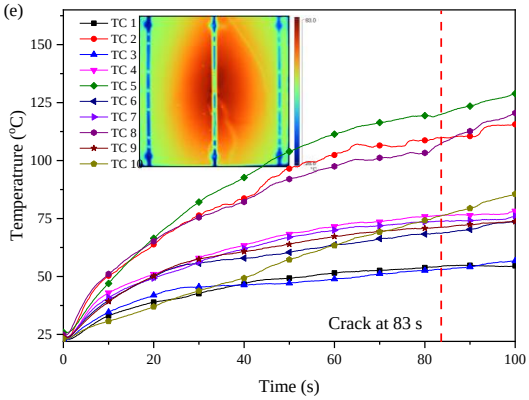

Fig. 5. The temperature variance at different monitoring points: (a) test 2, (b) test 6, (c) test 7, (d) test 10, and (e) test 13.

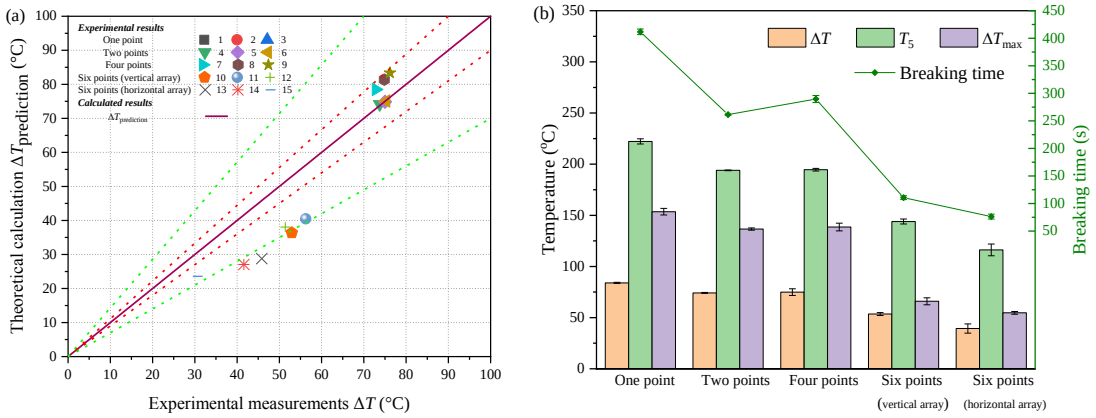

Fig. 6. The temperatures at the time of first crack occurrence. (a) Comparison of the temperature difference between theoretical calculation and test results with ± 10 % and ± 30 % reference lines for various types of point-supported glass facades. (b) Some significant temperatures with a standard error at the first breaking time.

4 Numerical results

4.1 Heat transfer model validation

The accuracy of the heat transfer model is verified by comparing the differences between temperatures measured by a thermocouple (TC 10) and calculated temperature by COMSOL, as shown in Fig. 7. It is found that the heat transfer model has been proved quite precise, with the maximum 18.3 % error, to predict the temperature distribution, especially considering the uncertainty of TCs estimated at 10-20 % [32].

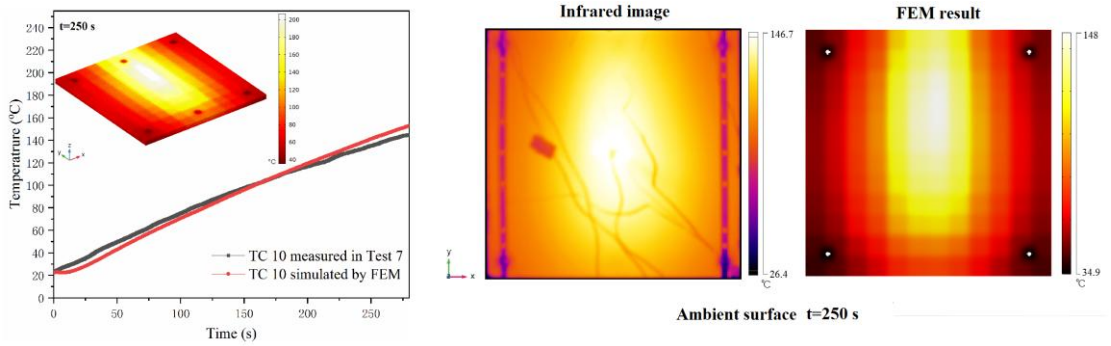

Fig. 7. Comparison of temperature variation between simulation and experiment in Test 7.

4.2 Stress distribution and breaking time prediction

Thermal stress is calculated based on the temperature distribution obtained from finite element analysis. It is found that, due to different installation forms, the stress distribution of various types of point-supported glass facades are quite distinct, and then results in the difference in breaking time. As shown in Fig. 8, the simulated breaking times are 256, 263, 117, and 97 s, which are in good agreement with averaged experimental results with 261, 289, 111, and 76 s, respectively. The differences are allowable which could be attributed to the slight difference in thermal loading between the experiments and simulations. Although the edges of glass panels are finely polished before experiments, they still have numerous minor imperfections and defects caused by drilling during manufacturing and installing procedures, which will result in the variation in tensile and compressive strength [23]. With regard to the stress field, as illustrated in Fig. 9, it is found that the maximum of first principal stresses locates at the edges of fixed points, which indicates that various constraints at the fixed points have a significant influence on the first principal stresses and further explain why cracks always initiate at the edges of fixed points during the experiments. It should be noted that, for the two-point-supported glass facades, the upper middle edge also existed relatively large stress except the region of fixed points surrounding, which results in that the cracks may initiate from this position. In addition, an interesting crack propagation phenomenon is observed during experiments with vertical arrangement. As shown in Fig. 10 (a), the cracks always initiate from the fixed points (D or F) on the left and right sides of the glass pane median line and rapidly form one or more approximately horizontal penetration cracks. For horizontal arrangement, as illustrated in Fig. 10 (b), all cracks initiate from B or H and rapidly forms one or more approximately vertical cracks through the glass pane. Because the length and width of the glass pane are much larger than the thickness (ratio: 100:1), the three-dimensional glass pane can be assumed to be a two-dimensional plate. Therefore, the present crack propagation behavior can be attributed to that, on the *xoy* plane where the glass exposed surface is located, for vertical arrangement, the maximum first principle stress is located at the edge of fixed point B, when the

rupture occurs, the cracks are prone to initiate from the edge of fixed point B, and due to the stress in the *y*-direction (σ_{yy}=43.1 MPa) is greater than the stress in the *x*-direction (σ_{xx} =42.4 MPa), thus the direction of the crack will be perpendicular to the *y*-direction, while for horizontal arrangement, the stress in the *x*-direction (σ_{xx}=59.9 MPa) is greater than the stress in the *y*-direction (σ_{yy} =45.6 MPa), and the direction of the crack will be perpendicular to the *x*-direction. In general, these numerical results further demonstrate that various types of installations have a significant effect on the thermal stress distribution of the point-supported glass facades, resulting in a large difference in the first breaking time and the fracture behavior and can deepen our understanding of the thermal feedback of point-supported glass facades.

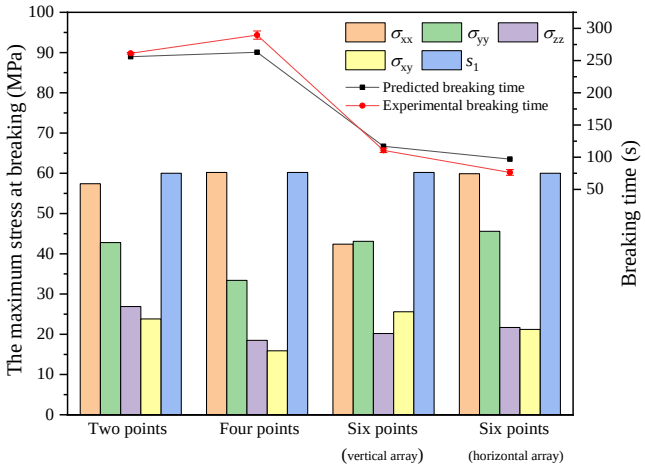

Fig. 8. The comparison maximum stress of various types of point-supported glass facades at breaking and breaking time between predicted and experimental results.

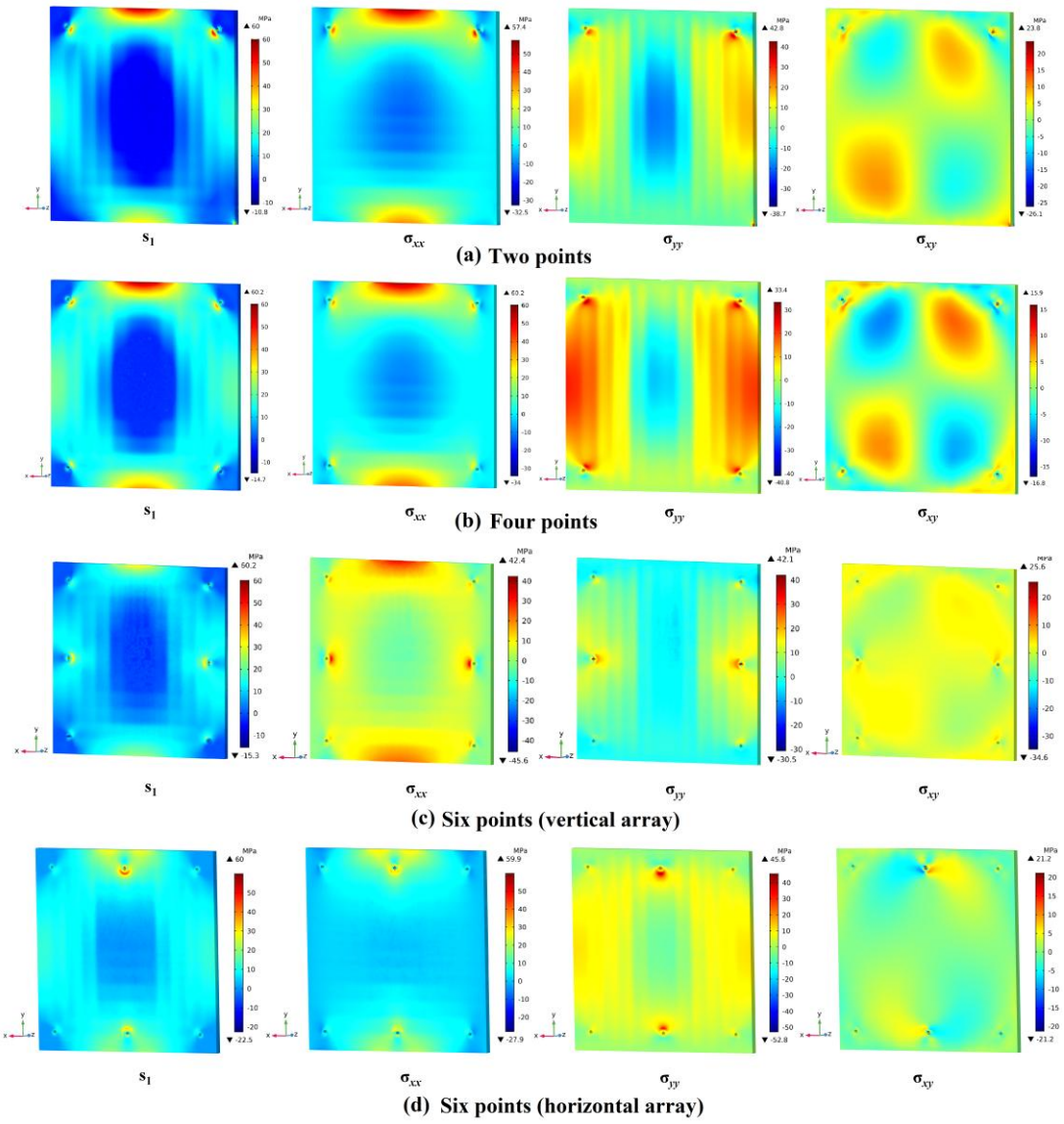

Fig. 9. The first principal stress ($\mathbf{s_1}$), stress tensor, x component ($\boldsymbol{\sigma_{xx}}$), stress tensor, y component ($\boldsymbol{\sigma_{yy}}$), and stress tensor, xy component ($\boldsymbol{\sigma_{xy}}$) field just before the first breaking.

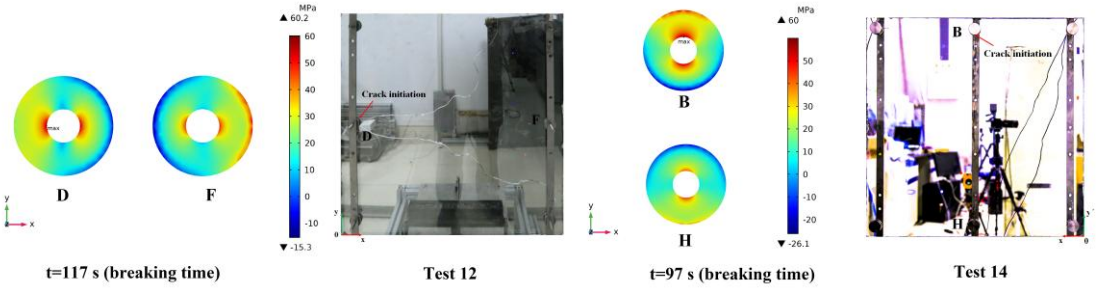

Fig. 10. The typical stress distribution at fixed points at breaking time and corresponding crack propagation path for six-point-supported glass facades.

4.3 Thermal resistance optimization

4.3.1 Optimization theoretical basis

The present experiments show that various installation forms have a great impact on thermal response and are crucial to breaking time. Determining the position of fixed points in which make the facades have best fire-resistance performance is still great difficult at present due to a large number of repeated experiments require a lot of manpower and financial resources for specific types of glass facades. Our previous works [33], concerning the variation of the first breaking time when the support points changed along the diagonal direction at distance from 50 mm to 500 mm for four-point-supported glass facades, demonstrated that the breaking time was first shortened and then increased which indicated that there existed a position in which the glass facades had the best fire performance. Therefore, based on the above precise heat transfer and thermal stress model, we adopted optimization method to determine the position of fixed points where various types of glass facades were subject to the minimum first principal stress. In the present study, Bound Optimization by Quadratic Approximation (BOBYQA) was performed [34]. The basic idea of the method is to iteratively approximate the objective function by a quadratic model which is valid in a region around the current iterate, the so-called trust region. The quadratic model is updated by minimizing the Frobenius norm of the difference in the Hessians of the two consecutive quadratic approximations [30] and it stops iterating as soon as no improvement over the current best estimate can be found with steps in the scaled control variables of a relative size larger than or equal to the optimality tolerance. As a parameter to be optimized, the distance from the center of the holes to the edge of the glass was set as L within the initial value of 35 mm, and the optimized interval was set in the range of 35 to 270 mm according to actual engineering situation. In addition, the default value of the optimality tolerance and the maximum number of model evaluations were set to 0.001 and 1000. The procedure of the optimization is shown in Fig. 11.

4.3.2 Optimization results

The results demonstrate that the optimization value of L, subjected to the minimum first principal stress, are 148.48, 221.25, 77.67, and 81.73 mm with the first principal stress of 57.25, 54.6, 52.5, and 48.4 MPa for two-point, four-point, six-point (vertical array), and six-point (horizontal array) supported glass facades respectively, which significantly decrease compared to the previous numerical results (L=55.00 mm) with the first principal stress of 60.0, 60.2, 60.2, and 60.0 MPa at breaking time, suggesting that the glass facades with these positions of fixed points have a better fire-resistance performance. In general, the optimization progress and numerical results could provide a reference for the optimization of fire protection performance of glass facade in engineering practice.

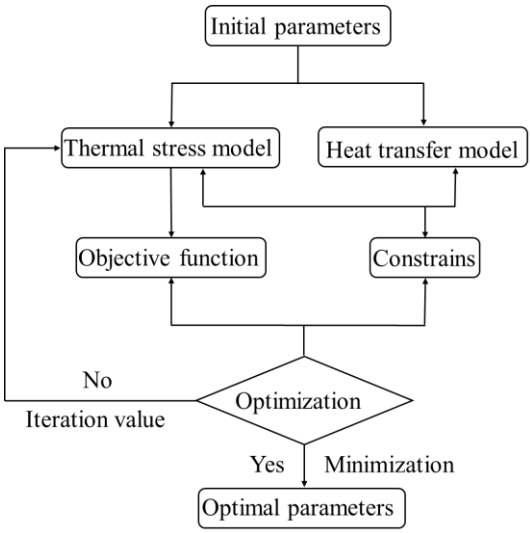

Fig. 11. The procedure of optimization based on heat transfer and thermal stress models.

Conclusions

To summarize, we investigated the effect of various installation forms on breaking behavior for point-supported glass facades using experimental study and numerical simulation. The results suggested that the design of point-supported glass facades need to take into consideration thermal resistance aspects to ensure safer structural performance. The insights gained from the present study aid the understanding of glass breaking mechanisms, providing the guidance schemes of safer point-supported glass facades, and developing the optimization tools for the position of fixed points. The main findings can be summarized as follow:

1. The first breaking times were distributed extensively in the range of 68-421 s, which demonstrated that the various types of installation forms had a significant impact on the thermal response of glass facades.
2. The results illustrate that the one-point-supported glass facades had the longest time with 412 s for the first crack occurrence whereas the glass eventually fell completely out of the frame. However, the six-point-supported glass facades had the shortest first breaking time with 76 s, but ultimately no glass pieces fell out of the frame.
3. With regard to six-point-supported glass facades, for vertical arrangement, the cracks always initiated from the fixed points on the left or right sides of glass pane median line and rapidly form one or more approximately horizontal penetration cracks while, for horizontal arrangement, all cracks were initiated from fixed points on the upper or lower center of glass pane and then rapidly formed one or more approximately vertical cracks through the glass pane,
4. The simulated breaking times are 256, 263, 117, and 97 s, which are in good agreement with averaged experimental results with 261, 289, 111, and 76 s,

459 respectively. We further carried out optimization simulation using bound
460 optimization by quadratic approximation method to make various types of
461 point-supported glass facade have a better thermal resistance performance.
462
463 **Conflict of interest**
464 The authors declare that there are no conflicts of interest.
465
466 **Acknowledgment**
467 This work is supported by the National Key Research and Development Plan of
468 China (Grant No. 2016YFC0800100), the National Natural Science Foundation of
469 China (Grant Nos. 51578524 and 51808523), the Fundamental Research Funds for the
470 Central Universities of China (Grant No. WK2320000038), and China Postdoctoral
471 Science Foundation Project (Project no. 2017M612093). The authors also sincerely
472 thank Mr. Mi Li, Mr. Lu Liu, and Mr. Fuhai Gou for their help during the
473 experiments.
474
475 **References**
476 [1] X. Wang, Q. Tan, Z. Wang, X. Kong, H. Cong, Preliminary study on fire protection of
477 window glass by water mist curtain, Int. J. Therm. Sci. 125 (2018) 44-51.
478 [2] S. Dembele, R. A. F. Rosario, J. X.Wen, Thermal breakage of window glass in room fires
479 conditions-Analysis of some important parameters, Building Environ. 54 (2012) 61-70.
480 [3] C. Bedon, X. Zhang, F. Santos, D. Honfi, M. Kozłowski, M. Arrigoni, L. Figuli, D. Lange,
481 Performance of structural glass facades under extreme loads-Design methods, existing
482 research, current issues and trends, Construct. Build. Mater. 163 (2018) 921-937.
483 [4] M. Li, L. Jiang, J. He, J. Sun, Kinetic triplet determination and modified mechanism function
484 construction for thermo-oxidative degradation of waste polyurethane foam using
485 conventional methods and distributed activation energy model method, Energy 175 (2019)
486 1-13.
487 [5] M. Debuyser, J. Sjöström, D. Lange, D. Honfi, D. Sonck, J. Belis, Behaviour of monolithic
488 and laminated glass exposed to radiant heating, Construct. Build. Mater. 130 (2017) 212-229.
489 [6] H. W. Emmons. The needed fire science. In: C. E. Grant, P. J. Pagni, editors. Fire Safety
490 Science–Proceedings of the First International Symposium. Berkeley, USA: Hemisphere
491 Publishing Corp.; 1986. pp. 33-53.
492 [7] P. Pagni, Thermal glass breakage, in: Fire Safety Science-Proceedings of the Seventh
493 International Symposium, IAFSS, Worcester, Massachusetts, USA,2002, pp. 3–22.
494 [8] O. Keski-Rahkonen. Breaking of window glass close to fire. Fire Mater. 12 (1988) 61-69.
495 [9] O. Keski-Rahkonen. Breaking of window glass close to fire, II: circular panes. Fire Mater. 15
496 (1991) 11-16.
497 [10] P. J. Pagni, A. A. Joshi. Glass breaking in fires. Fire Saf. Sci. 3 (1991) 791-802.
498 [11] Joshi AA, Pagni PJ. Fire-induced thermal fields in window glass. I—theory. Fire Saf. J. 22
499 (1994) 25-43.
500 [12] S. Dembele, R. Rosario, J. X. Wen. Investigation of glazing behavior in a fire environment

using a spectral discrete ordinates method for radiative heat transfer. Numer. Heat. Tr. B-Fund. 52 (2007) 489-506.
[13] K. Kang. Assessment of a model development for window glass breakage due to fire exposure in a field model. Fire Saf. J. 44 (2009) 415-424.
[14] M. J. Skelly, R. J. Roby, C. L. Beyler. An experimental investigation of glass breakage in compartment fires. J. Fire. Prot. Eng. 3 (1991) 25-34.
[15] T. J. Shields, G. W. H. Silcock, M. Flood. Performance of a single glazing assembly exposed to a fire in the centre of an enclosure. Fire Mater. 26 (2002) 51-75.
[16] J. Shields, G. W. H. Silcock, F. Flood. Behaviour of double glazing in corner fires. Fire Technol. 41 (2005) 37-65.
[17] A. A. Joshi, P. J. Pagni. User's guide to BREAK1, the Berkeley algorithm for breaking window glass in a compartment fire. Gaithersburg: NIST; 1991.
[18] M. Kozłowski, C. Bedon, D. Honfi. Numerical analysis and 1D/2D sensitivity study for monolithic and laminated structural glass elements under thermal exposure. Materials 11(8) (2018) 1447.
[19] C. Bedon, C. Louter. Thermo-mechanical Numerical Modelling of Structural Glass under Fire-Preliminary Considerations and Comparisons, Challenging Glass Conference Proceedings. 6(2018) 513-524.
[20] W. Lu, Y. Wang, H. Chen, L. Jiang, Q. Duan, M. Li., Q. Wang, J. Sun, Investigation of the thermal response and breakage mechanism of point-supported glass facade under wind load. Construct. Build. Mater. 186 (2018), 635-643.
[21] W. Lu, H. Chen, Y. Wang, Q. Duan, L. Jiang, Q. Wang, J. Sun, Study of point-supported glass breakage behavior with varying point-covered areas under thermal loading, Int. J. Therm. Sci. 132 (2018) 65–75.
[22] S. Brohez, D. Christian, M. Guy. A two-thermocouples probe for radiation corrections of measured temperatures in compartment fires. Fire Saf. J. 39 (2004) 399-411.
[23] S. Dembele, R. A. F. Rosario, Q. Wang, P. D. Warren, J. X. Wen. Thermal and stress analysis of glazing in fires and glass fracture modeling with a probabilistic approach. Numer. Heat. Tr. B-Fund. 58 (2010) 419-439.
[24] W. Weibull, A statistical distribution function of wide applicability, Journal of Applied Mechanics-Transactions of the ASME 18 (1951) 293-297.
[25] L. Yu, F. Liu, T. Bejib, M. Weng, B. Merci, Experimental study of the effectiveness of air curtains of variable width and injection angle to block fire-induced smoke in a tunnel configuration, Int. J. Therm. Sci. 134 (2018) 13-26.
[26] K. Mcgrattan, S. Hostikka, R. Mcdermott, J. Floyd, C. Weinschenk, K. Overholt, Fire dynamics simulator User's guide, National Institute of Standards and Technology, Gaithersburg, Maryland, 2016.
[27] F. W. Mowrer, Window breakage induced by exterior fires, Proceedings of the Second International Conference on Fire Research and Engineering, Society of Fire Protection Engineers, Bethesda, MD, 1998.
[28] R. Gardon, A review of radiant heat transfer in glass, J. Am. Ceram. Soc. 44 (1961) 305-313.
[29] K. Harada, A. Enomoto, K. Uede, T. Wakamatsu, An experimental study on glass cracking and fallout by radiant heat exposure, in: Fire Safety Science-Proceedings of the Sixth International Symposium, IAFSS, 2000, pp. 1063-1074.

[30] A. Comsol, COMSOL Multiphysics User's Guide, Version: COMSOL 5.3, 2017.
[31] Q. Wang, Y. Wang, Y. Zhang, H. Chen, J. Sun, L. He, A stochastic analysis of glass crack initiation under thermal loading, Appl. Therm. Eng. 67 (2014) 447-457.
[32] S.L. Manzello, R.G. Gann, S.R. Kukuck, K.R. Prasad, W.W. Jones, An experimental determination of a real fire performance of a non-load bearing glass wall assembly, Fire Technol. 43 (1) (2007) 77–89.
[33] Y. Wang, Q. Wang, G. Shao, H. Chen, Y. Su, J. Sun, L. He, K. M. Liew, Fracture behavior of a four-point fixed glass curtain wall under fire conditions. Fire Saf. J. 67 (2014) 24-34.
[34] M.J.D. Powell: The BOBYQA algorithm for bound constraint optimization without derivatives, Report DAMTP 2009/NA06, University of Cambridge, UK, 2009.